that a polymeric form of Sn(IV) may be generated in the oxidation of (P)SnS. Specifically, the reproducible value of 0.25 ± 0.02 electron abstracted is consistent with the formation of a Sn(IV) porphyrin tetramer with the stoichiometry $((P)Sn)_4S_3(ClO_4)_2$. This type of species should have wavelength maxima located between those of the original (P)SnS derivative and $(P)Sn(ClO_4)_2$, which is exactly what is observed. Unfortunately, all attempts to isolate or further characterize an oxidized form of (P)SnS have so far been unsuccessful.

(40) Cotton, F. A.; Wilkinson, G. *Advanced Inorganic Chemistry*; Wiley Interscience: New York, 1988; p 491.

Acknowledgment. The support of the CNRS and of the National Science Foundation (Grants CHE-8822881 and INT-8413696) is gratefully acknowledged.

Contribution from the Department of Chemistry, University of Houston, Houston, Texas 77204-5641, and Laboratoire de Synthèse et d'Electrosynthèse Organométallique Associé au CNRS (UA 33), Université de Bourgogne, Faculté des Sciences "Gabriel", 6 Boulevard Gabriel, 21100 Dijon, France

Effect of Pyridine Binding and Spin State on Spectroscopic and Electrochemical Properties of Phenyl- and (Perfluorophenyl)iron(III) Porphyrins

K. M. Kadish,*[1a] A. Tabard,[1b] W. Lee,[1a] Y. H. Liu,[1a] C. Ratti,[1a,b] and R. Guilard*[1b]

Received July 31, 1990

The effect of pyridine binding and spin state on the spectroscopic and electrochemical properties of six-coordinate σ-bonded iron(III) porphyrins is reported. The investigated compounds are represented by (P)Fe(R) where P is the dianion of octaethylporphyrin (OEP), tetraphenylporphyrin (TPP), tetra-*m*-tolylporphyrin (TmTP), tetra-*p*-tolylporphyrin (TpTP), or tetrakis(*p*-(trifluoromethyl)phenyl)porphyrin ($TpCF_3PP$) and R is C_6H_5, C_6F_4H, or C_6F_5. The five- and six-coordinate σ-bonded $(P)Fe(C_6H_5)$ derivatives are low spin in all solvents at room temperature. However, at 100 K in toluene, the ESR spectrum of $(TpCF_3PP)Fe(C_6H_5)$ is assigned as due to a mixture of the high- and low-spin-state Fe(III) complex. The five-coordinated $(P)Fe(C_6F_4H)$ and $(P)Fe(C_6F_5)$ derivatives are high spin in noncoordinating solvents, but low-spin coordinate iron(III) species are formed in neat pyridine or in pyridine/benzonitrile mixtures. The complexes were investigated by UV-visible, ^1H NMR, and ^{19}F NMR spectroscopy as well as by electrochemistry and provide the first examples for low-spin (perfluorophenyl)iron(III) porphyrin σ-bonded species. Formation constants for the addition of one pyridine ligand to high-spin $(P)Fe(C_6F_4H)$ and $(P)Fe(C_6F_5)$ were measured in benzonitrile, and these data are compared to related ligand-binding data for low-spin $(P)Fe(C_6H_5)$ derivatives under the same experimental conditions.

Introduction

A variety of σ-bonded iron(III) porphyrins have been synthesized and spectroscopically or electrochemically characterized[2-18] as model compounds in studies involving the metabolic reduction of polyhalogenated derivatives by cytochrome P_{450}.[18-20]

(1) (a) University of Houston. (b) Université de Bourgogne.
(2) Reed, C. A.; Mashiko, T.; Bentley, S. P.; Kastner, M. E.; Scheidt, W. R.; Spartalian, K.; Lang, G. *J. Am. Chem. Soc.* **1979**, *101*, 2948.
(3) Lexa, D.; Savéant, J.-M.; Battioni, J.-P.; Lange, M.; Mansuy, D. *Angew. Chem. Int. Ed. Engl.* **1981**, *103*, 6806.
(4) Clarke, D. A.; Dolphin, D.; Grigg, R.; Johnson, A. W.; Pinnock, H. A. *J. Chem. Soc. C* **1968**, 881.
(5) Lexa, D.; Mispelter, J.; Savéant, J.-M. *J. Am. Chem. Soc.* **1981**, *103*, 6806.
(6) Ortiz de Montellano, P. R.; Kunze, K. L.; Augusto, O. *J. Am. Chem. Soc.* **1982**, *104*, 3545.
(7) Lexa, D.; Savéant, J.-M. *J. Am. Chem. Soc.* **1982**, *104*, 3503.
(8) Ogoshi, H.; Sugimoto, H.; Yoshida, Z.-I.; Kobayashi, H.; Sakai, H.; Maeda, Y. *J. Organomet. Chem.* **1982**, *234*, 185.
(9) Mansuy, D.; Battioni, J.-P.; Dupré, D.; Sartori, E. *J. Am. Chem. Soc.* **1982**, *104*, 6159.
(10) Kunze, K. L.; Ortiz de Montellano, P. R. *J. Am. Chem. Soc.* **1983**, *105*, 1380.
(11) Battioni, P.; Mahy, J. P.; Gillet, G.; Mansuy, D. *J. Am. Chem. Soc.* **1983**, *105*, 1399.
(12) Cocolios, P.; Laviron, E.; Guilard, R. *J. Organomet. Chem.* **1982**, *228*, C39.
(13) Cocolios, P.; Lagrange, G.; Guilard, R. *J. Organomet. Chem.* **1983**, *253*, 65.
(14) Lançon, D.; Cocolios, P.; Guilard, R.; Kadish, K. M. *J. Am. Chem. Soc.* **1984**, *106*, 4472.
(15) Lançon, D.; Cocolios, P.; Guilard, R.; Kadish, K. M. *Organometallics* **1984**, *3*, 1164.
(16) Doppelt, P. *Inorg. Chem.* **1984**, *23*, 4009.
(17) Balch, A. L.; Renner, M. W. *Inorg. Chem.* **1986**, *25*, 303.
(18) Balch, A. L.; Renner, M. W. *J. Am. Chem. Soc.* **1986**, *108*, 2603.
(19) Uehleke, H.; Hellmer, K. H.; Tabarelli-Poplawski, S., *Arch. Pharmacol.* **1973**, *279*, 39.
(20) (a) Mansuy, D.; Nastainczyk, W.; Ullrich, V. *Arch. Pharmacol.* **1974**, *285*, 315. (b) Wolf, C. R.; Mansuy, D.; Nastainczyk, W.; Deutschmann, G.; Ullrich, V. *Mol. Pharmacol.* **1977**, *13*, 698.

The type of σ-bonded axial ligand and the porphyrin ring basicity will both influence the spin state of the iron(III) atom,[12-15,17,21,22] and this will be reflected in the spectroscopic or electrochemical properties of a given σ-bonded complex.

σ-Bonded phenyl[13,14,21] and tolyl[17] porphyrin complexes are low spin at room temperature in benzene or chloroform, while σ-bonded perfluorophenyl (C_6F_5 and C_6F_4H) derivatives of octaethyl- and tetraphenylporphyrins are high spin under the same experimental conditions.[21,22] Six-coordinate $(P)Fe(C_6H_5)(L)$ derivatives, where P is the dianion of a given porphyrin ring and L is a nitrogenous base, are also low spin,[15,17] but characterization of spin state in six-coordinate $(P)Fe(C_6F_5)(L)$ or $(P)Fe(C_6F_4H)(L)$ has never been reported.

As will be demonstrated in this paper, the binding of pyridine to high-spin $(P)Fe(C_6F_5)$ or $(P)Fe(C_6F_4H)$ produces a six-coordinate species that is accompanied by a change of spin state according to the following equation:

$$(P)Fe(R)_{hs} + py \rightleftharpoons (P)Fe(R)(py)_{ls} \quad (1)$$

The resulting six-coordinate complexes are low spin at all temperatures and provide the first examples for low-spin (perfluorophenyl)iron(III) σ-bonded porphyrins.

Previous electrochemical studies have shown that all low-spin $(P)Fe(C_6H_5)$ complexes are relatively stable upon electroreduction,[14,15,22] while all high-spin $(P)Fe(C_6F_5)$ and $(P)Fe(C_6F_4H)$ derivatives undergo a rapid cleavage of the iron–carbon bond upon the addition of one electron.[22] This difference in stability between the phenyl and perfluorophenyl σ-bonded complexes was attributed to the different spin states of the Fe(III) central metals but may also be due to the different axial ligands. This is explored in the present paper, which characterizes electrochemistry of various

(21) Tabard, A.; Cocolios, P.; Lagrange, G.; Gerardin, R.; Hubsch, J.; Lecomte, C.; Zarembowitch, J.; Guilard, R. *Inorg. Chem.* **1988**, *27*, 110.
(22) Guilard, R.; Boisselier-Cocolios, B.; Tabard, A.; Cocolios, P.; Simonet, B.; Kadish, K. M. *Inorg. Chem.* **1985**, *24*, 2509.

0020-1669/91/1330-1542$02.50/0 © 1991 American Chemical Society

six-coordinate (P)Fe(R)(py) derivatives in pyridine and pyridine/benzonitrile mixtures.

The investigated compounds are represented by (P)Fe(R), where P = the dianion of octaethylporphyrin (OEP), tetraphenylporphyrin (TPP), tetra-*m*-tolylporphyrin (TmTP), tetra-*p*-tolylporphyrin (TpTP), or tetrakis(*p*-(trifluoromethyl)phenyl)porphyrin ($TpCF_3PP$) and R = C_6H_5, C_6F_4H, or C_6F_5. Each iron(III) complex was also spectroscopically characterized by ^1H NMR, ^{19}F NMR, ESR, and UV–visible spectroscopy.

The derivatives in the $TpCF_3PP$ series were synthesized in order to extend the range of porphyrin macrocycle basicity from that of the previously investigated OEP or TPP derivatives and also to more completely investigate the effect of porphyrin ring basicity on the spectroscopic and electrochemical properties of the various complexes. The $TpCF_3PP$ macrocycle is less basic than OEP, TPP, TmTP, or TpTP and, for the case of $(TpCF_3PP)Fe(C_6F_5)$ and $(TpCF_3PP)Fe(C_6F_4H)$, provides the first examples where the porphyrin ring and the σ-bonded axial ligand both contain electron-withdrawing substituents.

Experimental Section

Chemicals. Synthesis and handling of each σ-bonded porphyrin was carried out in Schlenk tubes under an inert argon atmosphere. All solvents were distilled under argon from solutions containing CaH_2 (for CH_2Cl_2), benzophenone/sodium (for benzene and heptane), or P_2O_5 (for benzonitrile). Tetra-*n*-butylammonium hexafluorophosphate, $TBA(PF_6)$, was purchased from Fluka Corp., twice recrystallized from ethyl acetate, and dried in a vacuum oven at 40 °C prior to use.

Preparation of Compounds. $(TpCF_3PP)FeCl$,[23] (P)Fe(Cl),[23] and (P)Fe(R),[22] where P = OEP, TPP, TmTP, or TpTP and R = C_6F_4H, C_6F_5, or C_6H_5, were prepared as described in the literature.

$(TpCF_3PP)Fe(C_6H_5)$. A benzene solution of phenylmagnesium bromide was added dropwise via a syringe to 500 mg of $(TpCF_3PP)FeCl$ (0.51 mmol) in 200 mL of freshly distilled benzene. The reaction mixture was hydrolyzed with 30 mL of deaerated distilled water, after which the organic layer was washed twice with water, the two layers were separated, and the solution was dried over $MgSO_4$. After filtration, the dry benzene solution was rapidly passed through a short column of basic alumina using benzene as eluent. The solvent was removed by evaporation under reduced pressure. Recrystallization of the obtained solid in a benzene/heptane mixture gave 280 mg of $(TpCF_3PP)Fe(C_6H_5)$ (yield: 54%). EIMS, *m/z* (assignment, relative intensity in %): 1017 ($M^{\cdot+}$, 17.0), 1016 ($[M - H]^+$, 28.5), 941 ($[M - C_6H_5 + H]^{\cdot+}$, 57.8), 940 ($[M - C_6H_5]^+$, 100.0). ESR (toluene, 100 K): 1.94 (g_x), 2.30 (g_y), 2.52 (g_z), 5.79 ($g_\perp$), 2.00 ($g_\parallel$). Anal. Calcd for $C_{54}H_{29}N_4F_{12}Fe$: C, 63.71; H, 2.87; N, 5.51; Fe, 5.50. Found: C, 63.7; H, 2.8; N, 5.4; Fe, 5.3.

$(TpCF_3PP)Fe(C_6F_4H)$. A 1-equiv amount of (2,3,5,6-tetrafluorophenyl)magnesium bromide in benzene was added dropwise in the dark to 500 mg of $(TpCF_3PP)FeCl$ (0.51 mmol) in 200 mL of benzene, and the mixture was allowed to stand for 48 h. The reaction medium was hydrolyzed with 30 mL of deaerated water until neutrality and then dried over $MgSO_4$. After filtration, the solution was concentrated by evaporation of the benzene under reduced pressure and chromatographed in the dark over a basic alumina column using benzene as eluent. The obtained red solid was recrystallized from a toluene/heptane mixture and gave 239 mg of $(TpCF_3PP)Fe(C_6F_4H)$ (yield: 43%). EIMS, *m/z* (assignment, relative intensity in %): 1089 ($M^{\cdot+}$, 3.0), 1090 ($[M + H]^+$, 1.4), 1088 ($[M - H]^+$, 3.5), 940 ($[M - C_6F_4H]^+$, 100.0). ESR (toluene, 100 K): 5.79 ($g_\perp$), 2.00 ($g_\parallel$). Anal. Calcd for $C_{54}H_{25}N_4F_{16}Fe$: C, 59.50; H, 2.31; N, 5.14; Fe, 5.14. Found: C, 59.5; H, 2.6; N, 5.2; Fe, 5.1.

$(TpCF_3PP)Fe(C_6F_5)$. A 1-equiv amount of (pentafluorophenyl)magnesium bromide in benzene was added dropwise in the dark to 500 mg of $(TpCF_3PP)FeCl$ (0.51 mmol) in 200 mL of benzene and treated as described above for $(TpCF_3PP)Fe(C_6F_4H)$. Recrystallization gave 227 mg of $(TpCF_3PP)Fe(C_6F_5)$ (yield: 45%). EIMS, *m/z* (assignment, relative intensity in %): 1107 ($M^{\cdot+}$, 3.8), 1108 ($[M + H]^+$, 1.9), 941 ($[M - C_6F_5 + H]^{\cdot+}$, 82.2), 940 ($[M - C_6F_5]^+$, 100.0). ESR (toluene, 100 K): 5.78 ($g_\perp$), 1.99 ($g_\parallel$). Anal. Calcd for $C_{54}H_{24}N_4F_{17}Fe$: C, 58.56; H, 2.18; N, 5.06; Fe, 5.04. Found: C, 58.5; H, 2.2; N, 4.2; Fe, 4.2.

Physicochemical and Electrochemical Measurements. Elemental analyses were performed by the "Service de Microanalyse du CNRS". Mass spectra were recorded in the electron-impact mode with a VG 70-70 spectrometer (ionizing energy 70 eV, ionizing current 0.2 mA, source temperature 250–500 °C). ^1H and ^{19}F NMR spectra were recorded at 400.13 and 376.48 MHz, respectively, on a Bruker WM 400 spectrometer of the "Centre de Résonance Magnétique" at the University of Bourgogne. Spectra were measured in 0.5 mL of C_6D_6, C_7D_8, or C_6D_5N by using tetramethylsilane (^1H NMR) or fluorotrichloromethane (^{19}F NMR) as a reference. ESR spectra were recorded at 100 K in frozen solution with a Bruker ESP 300 spectrometer. Electronic absorption spectra were recorded with a Perkin-Elmer 559 spectrophotometer, a Tracor Northern Model 6500 rapid-scanning spectrometer, or an IBM Model 9430 spectrophotometer.

Cyclic voltammograms were recorded with a three-electrode system using an EG&G Model 174A potentiostat coupled with an EG&G Model 175 universal programmer or an IBM EC 225 voltammetric analyzer. Bulk controlled-potential coulometry was performed with an EG&G Model 173 potentiostat–galvanostat. Thin-layer spectroelectrochemical measurements were performed with an EG&G Model 173 potentiostat that was coupled with a Tracor Northern Model 6500 rapid-scanning spectrometer.

Results and Discussion

Spectral Characterization of Five-Coordinate $(TpCF_3PP)Fe(R)$. The $(TpCF_3PP)Fe(R)$ complexes were synthesized for the first time as part of this present study. Elemental analyses and mass spectral data are given in the Experimental Section and are consistent with the expected molecular formulas. The parent peak for each $(TpCF_3PP)Fe(R)$ complex corresponds to the ionic $[(TpCF_3PP)Fe]^+$ fragment. The relative intensity of the molecular peak is 3.0% for $(TpCF_3PP)Fe(C_6F_4H)$ and 3.8% for $(TpCF_3PP)Fe(C_6F_5)$, both of which are weaker than the molecular peaks of $(P)Fe(C_6F_4H)$[22] or $(P)Fe(C_6F_5)$,[22] where P = OEP (21–22%), TPP (19–22%), TmTP (30%), or TpTP (22–25%). The relative molecular peak intensity of 17.0% for $(TpCF_3PP)Fe(C_6H_5)$ is also less than the relative molecular peak intensities of 50–60% for $(P)Fe(C_6H_5)$,[13] where P = OEP, TPP, TmTP, or TpTP. This suggests a weaker iron–carbon bond in $(TpCF_3PP)Fe(R)$ than in other previously investigated (P)Fe(R) species, where R = C_6H_5, C_6F_4H, or C_6F_5.

The UV–visible data for $(TpCF_3PP)Fe(C_6H_5)$ in benzene are given in Table I. The complex has a single intense Soret band at 410 nm and two Q bands at 521 and 548 nm and is characteristic of a low-spin σ-bonded Fe(III) porphyrin complex. This spectrum is similar to the spectrum of $(TPP)Fe(C_6H_5)$ (λ_{max} = 408, 518, 548 nm) and $(TmTP)Fe(C_6H_5)$ (λ_{max} = 408, 518, 550 nm),[13] both of which are low spin at room temperature. In contrast, the UV–visible spectra of $(TpCF_3PP)Fe(C_6F_4H)$ and $(TpCF_3PP)Fe(C_6F_5)$ in benzene are both typical of high-spin Fe(III) porphyrins. The Soret band is located at 414 nm (R = C_6F_4H) or 416 nm (R = C_6F_5), and these values may be compared to the bands for $(TPP)Fe(C_6F_4H)$ and $(TPP)Fe(C_6F_5)$, which are both located at 417 nm.[22] The perfluorophenyl porphyrin derivatives have an additional band between 367 and 369 nm, which confers a slight hyperporphyrin character to the species. There is also an intense Q band centered at 512 nm, which is typical[24] of a high-spin Fe(III) porphyrin. In addition, the $TpCF_3PP$ perfluorophenyl σ-bonded species have a metal to ligand charge-transfer band that is located at 709–710 nm (see Table I) and this band is not found in the low-spin C_6H_5 species.

The ^1H NMR spectra of $(TpCF_3PP)Fe(C_6H_5)$ in benzene-d_6 and pyridine-d_5 confirm the above iron spin states. The pyrrole proton signal of low-spin $(TpCF_3PP)Fe(C_6H_5)$ in benzene is centered at −17.97 ppm (see Table II) and differs substantially from the pyrrole proton signal of high-spin $(TpCF_3PP)FeCl$, which is located at ≈ +83 ppm.[25] $(TpCF_3PP)Fe(C_6F_5)$ and $(TpCF_3PP)Fe(C_6F_4H)$ (Figure 1a and Table II) have pyrrole signals located at 66.67 and 62.32 ppm in C_6D_6, and these are similar to signals for the same proton groups of high-spin $(TpCF_3PP)FeCl$ under the same solution conditions.[25-28] The

(23) Buchler, J. W. In *The Porphyrins*; Dolphin, D., Ed.; Academic: New York, 1978; Vol. I, Chapter 10.

(24) Gouterman, M. In *The Porphyrins*; Dolphin, D., Ed.; Academic: New York, 1978; Vol. III, Chapter 1.

(25) ^1H NMR data of $(TpCF_3PP)FeCl$ (C_6D_6; 294 K; δ, ppm): 83.02 (8 H, broad s, pyrr H), 8.41 and 5.10 (8 H, broad s, *o*-H and *o'*-H), 12.80 and 11.68 (8 H, s, *m*-H and *m'*-H).

(26) La Mar, G. N.; Walker, F. A. In *The Porphyrins*; Dolphin, D., Ed.; Academic: New York, 1979; Vol. IV, Chapter 2.

(27) Walker, F. A.; La Mar, G. N. *Ann. N.Y. Acad. Sci.* **1973**, *206*, 328.

(28) La Mar G. N.; Eaton, G. R.; Holm, R. H.; Walker, F. A. *J. Am. Chem. Soc.* **1973**, *95*, 63.

Table I. UV–Visible Data for $(TpCF_3PP)Fe(R)$ Complexes in Several Solvents

ax ligand, R	solvent[a]	electrode reacn	λ_{max}, nm (10^{-3} ϵ, $M^{-1}\cdot cm^{-1}$)						
C_6H_5	benzene	none		410 (98)		521 (11.0)	548 (5.7)		
	benzonitrile	none		412 (105)		518 (8.7)	554 (6.4)	608 (3.3)	
	pyridine	none		428 (105)		531 (9.9)	565 (5.0)	609 (3.2)	
	pyridine	1st redn	364 (35)	426 (90)	452 (65)	531 (19.7)	556 (sh)		
C_6F_4H	benzene	none	369 (63)	414 (88)		512 (12.8)	570 (3.2)		710 (3.6)
	benzonitrile	none	370 (46)	421 (96)		514 (12.2)	567 (4.4)	620 (sh)	708 (3.0)
	pyridine	none		426 (142)			567 (sh)	628 (4.2)	
	pyridine	1st redn (1)[b]		426 (109)	446 (135)	534 (20.5)			
		1st redn (2)[c]		425 (168)	445 (sh)	530 (24.4)	557 (sh)		
	pyridine	2nd redn	379 (35)		450 (57)	532 (14.7)			729 (2.1)
	pyridine	3rd redn	366 (44)		464 (73)	531 (21.6)			
C_6F_5	benzene	none	367 (69)	416 (93)		512 (13.1)	568 (3.0)		709 (4.0)
	benzonitrile	none	366 (51)	421 (100)		513 (12.7)	571 (3.8)		709 (4.0)
	pyridine	none		426 (139)			567 (sh)	628 (3.9)	
	pyridine	1st redn		425 (187)		530 (24.5)	561 (sh)		
	pyridine	2nd redn	380 (sh)		447 (61)	530 (12.9)			729 (4.4)
	pyridine	3rd redn	365 (41)		465 (68)	531 (19.6)			

[a] Spectra in benzonitrile and pyridine were obtained in solutions containing 0.2 M $TBA(PF_6)$ as supporting electrolyte. [b] Spectrum obtained 40 s after electrolysis at −0.70 V. [c] Spectrum obtained 270 s after electrolysis at −0.70 V.

porphyrin phenyl meta-proton signals appear as two broad well-separated peaks at 10.41 and 11.10 ppm ($R = C_6F_4H$) or 10.77 and 11.48 ppm ($R = C_6F_5$), while the ortho-proton resonances range between 5.28 and 8.20 ppm. Both sets of protons are highly anisotropic in the limit of the slow phenyl-group rotation[29] due to the electronic effect from the electron-withdrawing CF_3 groups and clearly demonstrate that the Fe(III) atoms in $(TpCF_3PP)Fe(C_6F_4H)$ and $(TpCF_3PP)Fe(C_6F_5)$ are both pentacoordinated and out of the macrocyclic plane.

The ESR spectrum of $(TpCF_3PP)Fe(C_6H_5)$ in frozen toluene solution is characterized by two overlapping types of ESR signals. There are g_x, g_y, and g_z signals characteristic of a low-spin state Fe(III) complex as well $g_\parallel = 2$ and $g_\perp \approx 6$ values, which are characteristic of high-spin state Fe(III) species.[30] Similar ESR spectra have been reported for $(OEP)Fe(C_6H_5)$ and $(TPP)Fe(C_6H_5)$ at 100 K,[21] and these spectra were assigned as due to a mixture of the high- and low-spin-state Fe(III) complex.

The ESR spectra of $(TpCF_3PP)Fe(C_6F_4H)$ and $(TpCF_3PP)Fe(C_6F_5)$ differ from the spectrum of $(TpCF_3PP)Fe(C_6H_5)$ in that the first two complexes have axial symmetry ($g_\perp \approx 6$, $g_\parallel \approx 2$), confirming the presence of only high-spin-state Fe(III). Similar ESR spectra were previously reported for $(P)Fe(C_6F_5)$ and $(P)Fe(C_6F_4H)$ (P = OEP, TPP) under the same solution conditions.[21,22]

Spectral Characterization of Six-Coordinate (P)Fe(R)(py). The UV–visible spectrum of $(P)Fe(C_6F_4H)$ or $(P)Fe(C_6F_5)$ changes substantially upon going from benzene to pyridine, as shown in Table I. Neither compound has a ligand to metal charge-transfer band in pyridine, and under these solution conditions the species can be classified as having "normal" rather than "hyperporphyrin" spectra. A normal spectrum is obtained for low-spin $(P)Fe(C_6H_5)(py)$, and this suggests that the C_6F_5 and C_6F_4H derivatives can also be classified as low-spin-state species in neat pyridine.

A definitive low-spin state assignment for $(P)Fe(C_6F_5)(py)$ and $(P)Fe(C_6F_4H)(py)$ is given by ^1H NMR spectroscopy of the two complexes in C_5D_5N. These data are summarized in Table II, which also gives data for high-spin $(P)Fe(C_6F_5)$ and $(P)Fe(C_6F_4H)$ in C_6D_6. The ^1H NMR spectra of the perfluorophenyl derivatives change dramatically upon going from benzene-d_6 to pyridine-d_5 as solvent (see Figure 1 and Table II). The high-field shift of the pyrrole proton signal of $(P)Fe(C_6F_4H)(py)$ provides clear evidence for an alteration of the Fe(III) spin state, as shown in eq 1. The conversion of $(P)Fe(C_6F_4H)$ to $(P)Fe(C_6F_4H)(py)$ also results in a shift of the C_6F_4H *p*-proton signal, as shown in Figure 1.

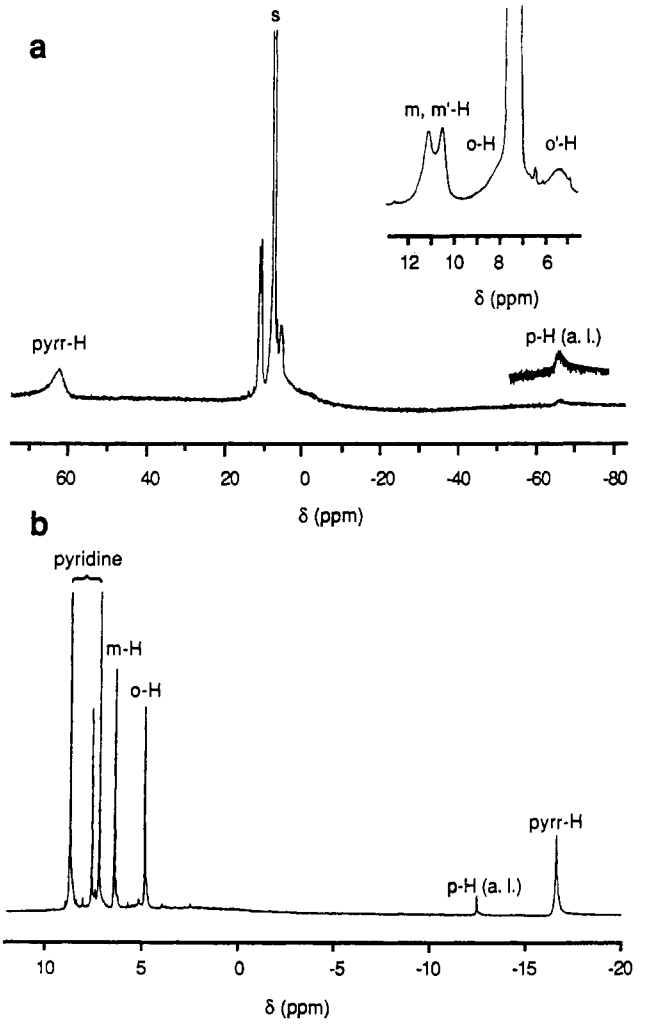

Figure 1. ^1H NMR spectra of $(TpCF_3PP)Fe(C_6F_4H)$ at 294 K in (a) C_6D_6 and (b) C_5D_5N. Resonances notated by "a.l." are those of the C_6F_4H axial ligand.

The five investigated $(P)Fe(C_6F_5)$ derivatives exhibit the same type of spectral changes upon coordination by pyridine, and each of the resulting six-coordinate complexes is assigned as containing a low-spin-state Fe(III) central metal. The spectral differences between the compounds in C_6D_6 and C_5D_5N are consistent with an alteration of the porphyrin symmetry upon going from (P)Fe(R) to (P)Fe(R)(py). The formation of a six-coordinate com-

(29) Eaton, S. S.; Eaton, G. R. *J. Am. Chem. Soc.* **1977**, *99*, 6594.
(30) Palmer, G. In *Iron Porphyrins*; Lever, A. B. P., Gray, H. B., Eds.; Addison-Wesley: Reading, MA, 1983; Part II, Chapter 2.

Table II. ^{1}H NMR Data[a] for the (OEP)Fc(R) and ($TpCF_3PP$)Fe(R) Complexes in C_6D_6 and in C_5D_5N

porphyrin, P	ax ligand, R	solvent	porphyrin protons	multi/intens	δ	ax ligand protons	multi/intens	δ
OEP	C_6H_5	C_6D_6[b]	α-CH_2	m/8	4.46	*o*-H	s/2	−79.90
			α′-CH_2	m/8	−1.70	*m*-H	s/2	13.23
			β-CH_3	t/24	−1.76	*p*-H	s/1	−23.80
			meso-H	s/4	5.53			
		C_5D_5N[c]	α-CH_2	m/8	0.07	*o*-H	s/2	−55.70
			α′-CH_2	m/8	−2.27	*m*-H	s/2	16.30
			β-CH_3	t/24	−4.06	*p*-H	s/1	−8.90
			meso-H	s/4	−3.23			
	C_6F_4H	C_6D_6[d]	α-CH_2	s/8	39.91	*p*-H	s/1	−58.85
			α′-CH_2	s/8	42.89			
			β-CH_3	t/24	5.88			
			meso-H	s/4	−48.56			
		C_5D_5N	α-CH_2	s/8	3.78	*p*-H	s/1	−9.49
			α′-CH_2	s/8	5.60			
			β-CH_3	t/24	−0.70			
			meso-H	s/4	1.94			
	C_6F_5	C_6D_6[d]	α-CH_2	s/8	41.71			
			α′-CH_2	s/8	42.69			
			β-CH_3	t/24	6.19			
			meso-H	s/4	55.01			
		C_5D_5N	α-CH_2	m/8	4.18			
			α′-CH_2	m/8	5.81			
			β-CH_3	t/24	−0.58			
			meso-H	s/4	2.28			
$TpCF_3PP$	C_6H_5	C_6D_6	*o*-H	s/4	4.27	*o*-H	s/2	−84.27
			o′-H	s/4	2.47	*m*-H	s/2	13.12
			m-H	s/4	4.98	*p*-H	s/1	−30.22
			m′-H	s/4	4.63			
			pyrr H	s/8	−17.97			
		C_5D_5N	*o*-H	d/8	2.75	*o*-H	s/2	−58.85
			m-H	d/8	4.95	*m*-H	s/2	18.94
			pyrr H	s/8	−21.18	*p*-H	s/1	−13.40
	C_6F_4H	C_6D_6	*o*-H	s/4	7.97	*p*-H	s/1	−67.13
			o′-H	s/4	5.28			
			m-H	s/4	11.10			
			m′-H	s/4	10.41			
			pyrr H	s/8	62.32			
		C_5D_5N	*o*-H	d/8	4.90	*p*-H	s/1	−12.47
			m-H	d/8	6.42			
			pyrr H	s/8	−16.63			
	C_6F_5	C_6D_6	*o*-H	s/4	8.20			
			o′-H	s/4	5.38			
			m-H	s/4	11.48			
			m′-H	s/4	10.77			
			pyrr H	s/8	66.67			
		C_5D_5N	*o*-H	d/8	4.93			
			m-H	d/8	6.50			
			pyrr H	s/8	−16.43			

[a] Spectra recorded at 294 K with $SiMe_4$ as internal reference; chemical shifts (δ, ppm) downfield from $SiMe_4$ are defined as positive. Key: s = singlet; d = doublet; t = triplet; m = multiplet. [b] From ref 13. [c] From ref 15. [d] From ref 22.

plex will result in a displacement of the central Fe(III) atom into the plane of the porphyrin ring, which induces a lowering of the anisotropy between the two faces of the macrocycle. A similar lowering of anisotropy is also observed upon pyridine binding by the C_6H_5 derivatives, which do not undergo a change of spin state under NMR recording conditions. For example, ($TpCF_3PP$)-Fe(C_6H_5)(py) has a single broad peak for the meta protons at 4.95 ppm and a single peak for the ortho protons at 2.75 ppm.

The C_6H_5 para-proton signal of (P)Fe(C_6H_5) shifts downfield upon going from benzene-d_6 to pyridine-d_5, and this suggests a decrease of the metal–axial ligand electron transfer. This shift can be explained by the π-acceptor behavior of coordinated pyridine on the Fe(III) center of (P)Fe(C_6H_5)(py). The pyrrole protons of (P)Fe(C_6H_5)(py) appear as a singlet at ≈ −21 ppm in pyridine, and this value may be compared to a resonance at ≈ −18 ppm for (P)Fe(C_6H_5) in C_6D_6.

The conversion of (P)Fe(R) to (P)Fe(R)(py) was also monitored by UV–vis spectroscopy in benzonitrile containing pyridine and gave data of the type shown in Figure 2a for ($TpCF_3PP$)-Fe(C_6H_5). Peak maxima for absorption bands of the perfluorophenyl complexes shift toward the red upon going from benzonitrile to pyridine/benzonitrile mixtures, consistent with the binding of pyridine to give the six-coordinate low-spin complex.

The spectral changes in Figure 2a were analyzed as a function of pyridine concentration at 421 and 512 nm, and the resulting plot of log $[(A - A_\infty)/(A_0 - A)]$ vs log [py] gives a linear slope of 0.98 ± 0.01, as shown in Figure 2b. The zero intercept corresponds to a log β° = 3.5 ± 0.2, which is identical with the formation constant for addition of pyridine to high-spin ($TpCF_3PP$)Fe(C_6F_4H) under the same solution conditions (see later sections).

^{19}F NMR Spectroscopy. ^{19}F NMR spectral data of (P)Fe-(C_6F_4H)(py) and (P)Fe(C_6F_5)(py) in pyridine-d_5 are summarized in Table III. The axial fluorine ligands give two (C_6F_4H) or three (C_6F_5) singlet signals in the range −105.60 to −237.82 ppm with respect to the external $CFCl_3$ reference. As expected, the broadest peak is observed for the *o*-fluorine atoms and the narrowest for the *p*-fluorine atom [$\Delta H_{1/2} \approx 180$ Hz (*o*-F), 70 Hz (*m*-F), 40 Hz(*p*-F)]. The range of chemical shifts agrees with a paramagnetic low-spin iron(III) metal center coordinated to a C_6F_4H or C_6F_5 group. The covalent iron–axial ligand bond is extremely stable, and (P)$Fe^{II}(py)_2$ is not formed at room temperature in neat

Table III. ^{19}F NMR Data[a] for (P)Fe(R)

porphyrin, P	ax ligand, R	porphyrin fluorines				ax ligand fluorines			
			multi/intens	$(\Delta H/H)_{obsd}$	$(\Delta H/H)_{iso}$		multi/intens	$(\Delta H/H)_{obsd}$	$(\Delta H/H)_{iso}$
OEP	C_6F_4H					*o*-F	s/2	−116.71	8.76
						m-F	s/2	−213.57	−72.88
	C_6F_5					*o*-F	s/2	−112.26	11.99
						m-F	s/2	−236.30	−73.78
						p-F	s/1	−111.64	45.76
TPP	C_6F_5					*o*-F	s/2	−120.53	3.05
						m-F	s/2	−237.38	−75.69
						p-F	s/1	−110.45	45.65
TmTP	C_6F_5					*o*-F	s/2	−119.77	3.64
						m-F	s/2	−237.14	−75.52
						p-F	s/1	−110.49	45.59
TpTP	C_6F_5					*o*-F	s/2	−120.99	2.40
						m-F	s/2	−237.20	−75.46
						p-F	s/1	−111.36	44.91
$TpCF_3PP$	C_6H_5	CF_3	s/12	−62.85	−2.05				
	C_6F_4H	CF_3	s/12	−61.89	−1.03	*o*-F	s/2	−122.13	1.95
						m-F	s/2	−215.67	−76.95
	C_6F_5	CF_3	s/12	−61.86		*o*-F	s/2	−116.39	
						m-F	s/2	−237.82	
						p-F	s/1	−105.60	

[a] Spectra recorded in C_5D_5N at 294 K with $CFCl_3$ as external reference; chemical shifts downfield from $CFCl_3$ are defined as positive. Key: s = singlet.

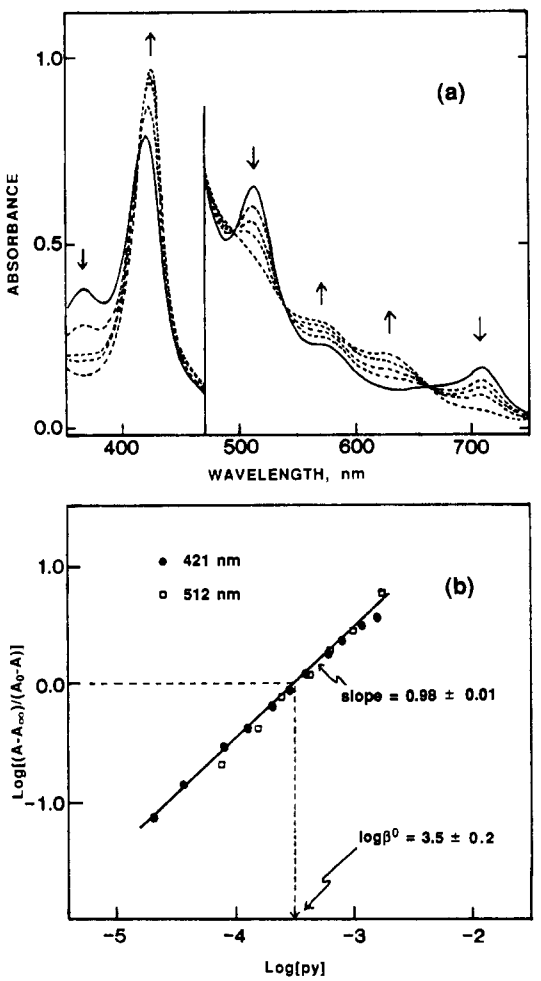

Figure 2. (a) Spectral changes associated with the conversion of $(TpCF_3PP)Fe(C_6F_5)$ to $(TpCF_3PP)Fe(C_6F_5)(py)$ in PhCN and (b) analysis of spectral data to obtain the pyridine binding constant.

pyridine, as is the case for $(P)Fe(C_6H_5)$.[15]

The shift of the *o*-fluorine resonance is small ($\Delta\delta \approx 8$ ppm), indicating that the porphyrin ring only slightly affects the ^{19}F resonances. On the other hand, the axial ligand induces a large change, as demonstrated by the downfield shift ($\Delta\delta \approx 23$ ppm) of the *m*-fluorine atoms upon going from the σ-bonded C_6F_4H to the σ-bonded C_6F_5 complexes (see Table III). This can be explained by the electron-withdrawing properties of the fluorine atoms.

The isotropic chemical shifts summarized in Table III were calculated by using diamagnetic isostructural $(P)In(C_6F_4H)$ or $(P)In(C_6F_5)$ as a reference.[31] The paramagnetic fluorine chemical shifts of the porphyrin CF_3 groups are low, and no effect of the axial ligand is observed. Similar results were reported for low-spin iron(III) derivatives with pyrrole-substituted CF_3 groups.[32] The paramagnetic fluorine chemical shifts were analyzed in a manner similar to that done for proton chemical shifts with two contributions (the Fermi contact and dipolar contributions),[26] and the resulting data indicate that either the fluorine contact and dipolar shifts have opposite signs or that the two contributions are very low. The later hypothesis could be rationalized by the fact that the *p*-$CF_3C_6H_4$ groups are orientated nearly perpendicular to the porphyrin plane, which would decrease the magnitude of the unpaired spin delocalization from the iron porphyrin ring. However, this is not the case for the pyrrole-substituted trifluoromethyl porphyrin complexes and a different spin delocalization mechanism must be invoked to explain the paramagnetic fluorine chemical shifts of such derivatives.

The axial fluorine isotropic chemical shifts show opposite signs compared to the axial phenyl proton resonances.[17,21] This result indicates that a similar $M \rightarrow L(\pi^*)$ charge transfer occurs for the σ-bonded phenyl and the perfluorophenyl complexes. It is estimated that fluorine contact interactions are much larger than proton contact interactions with the opposite sign if the π-electron spin distribution is constant.[33,34] According to these results, the data in Table III show that an axial coordination of pyridine modifies to a different extent the paramagnetic shifts of the phenyl protons[17,21] and perfluorophenyl fluorine atoms. The pyridine π-acceptor character must be lowered by the electron-withdrawing properties of the fluorine atoms. However, the coordination of pyridine as a sixth ligand induces a change from high-spin- to low-spin-state Fe(III) and the perfluorophenyl groups then act as high-field ligands. These results are unambiguously proven by the ^{19}F NMR data, which show for the first time that this type of measurement can be used to investigate electronic structures

(31) Tabard, A.; Guilard, R.; Kadish, K. M. *Inorg. Chem.* **1986**, *25*, 4277.
(32) Toi, H.; Homma, M.; Suzuki, A.; Ogoshi, H. *J. Chem. Soc., Chem. Commun.* **1985**, 1791.
(33) Icli, S.; Kreilick, R. W. *J. Phys. Chem.* **1971**, *75*, 3462.
(34) Espersen, W. G.; Kreilick, R. W. *Mol. Phys.* **1969**, *16*, 577.

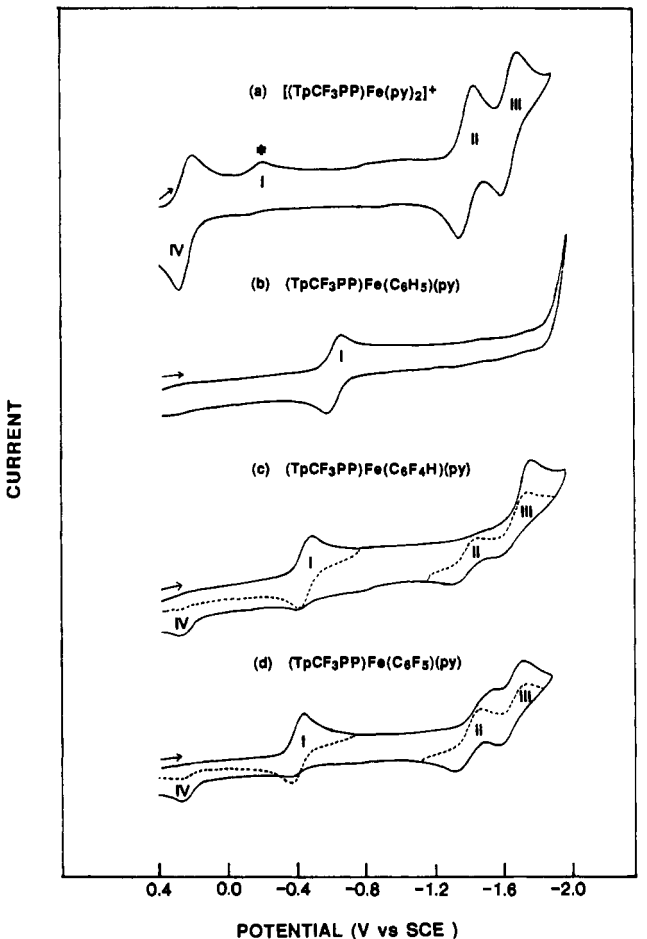

Figure 3. Cyclic voltammograms of (a) $(TpCF_3PP)FeCl$, (b) $(TpCF_3PP)Fe(C_6H_5)$, (c) $(TpCF_3PP)Fe(C_6F_4H)$, and (d) $(TpCF_3PP)Fe(C_6F_5)$ in pyridine, 0.2 M $TBA(PF_6)$. Scan rate = 0.1 V/s. The starred peak corresponds to a reduction of $(TpCF_3PP)FeCl(py)$ (see text).

of iron porphyrin complexes and related metalloenzymes.

Electrochemistry of $(TpCF_3PP)FeCl$ in Pyridine. The electrochemistry of various (P)FeCl complexes has been characterized under numerous solution conditions.[35-37] Reversible electroreductions are generally observed, and the electrode reactions correspond to the stepwise formation of an Fe(II), an Fe(I), and an Fe(I) anion-radical species.

The electrochemistry of $(TpCF_3PP)FeCl$ is virtually identical with what has been reported for (TPP)FeCl under similar solution conditions.[36,37] No oxidations are observed in pyridine, but three reversible reductions are located at 0.25, −1.37, and −1.62 V, as shown in Figure 3a. The reactions labeled as IV, II, and III correspond to the stepwise reduction of $[(P)Fe(py)_2]^+$, $(P)Fe(py)_2$, and $[(P)Fe]^-$ at the electrode surface. A small irreversible peak (reaction I) is also located at $E_p = -0.19$ V for a potential scan rate of 0.1 V/s, and this reaction is associated with the conversion of (P)FeCl(py) to $(P)Fe(py)_2$, as has been discussed in the literature for the case of (TPP)FeCl in pyridine.[36]

Electrochemistry of (P)Fe(R)(py). The electroreduction of $(OEP)Fe(C_6H_5)(py)$ and $(TPP)Fe(C_6H_5)(py)$ in pyridine or pyridine/benzonitrile mixtures has been described in the literature.[15] Both complexes undergo an one-electron reversible reduction which occurs at $E_{1/2} = -1.03$ V (P = OEP) or −0.76 V (P = TPP). Similar electrochemistry is observed for $(TpCF_3PP)Fe(C_6H_5)(py)$ (see Table IV), which is reduced at $E_{1/2} = -0.61$ V in pyridine, as shown in Figure 3b. The Soret band for this complex shifts from 412 to 431 nm after a one-electron reduction, and a new charge-transfer band appears at 769 nm. This suggests an involvement of both the metal and the porphyrin ring in the first reduction, as was reported for $[(OEP)Fe(C_6H_5)(py)]^-$ and $[(TPP)Fe(C_6H_5)(py)]^-$ in pyridine.[15]

Table IV. Half-Wave Potentials (V) of Various Investigated (P)FeCl and (P)Fe(R)(py) Complexes in Pyridine Containing 0.2 M $TBA(PF_6)$

		reduction		
porphyrin, P	non-py ligand	1st	2nd	3rd
OEP	Cl^- [a]	−0.02	−1.80 [b]	−1.90
	C_6F_5	−0.71 [b]	−1.82 [b]	
	C_6F_4H	−0.77 [b]	−1.82 [b]	−1.90
	C_6H_5 [c]	−1.03		
TpTP	Cl^- [a]	0.13	−1.49	−1.71
	C_6F_5	−0.53	−1.58 [b]	−1.70
	C_6F_4H	−0.58	−1.70 [b]	−1.71
TmTP	Cl^- [a]	0.15	−1.56 [b]	−1.72
	C_6F_5	−0.52	−1.56 [b]	−1.70
	C_6F_4H	−0.57	−1.68 [b]	−1.70
TPP	Cl^- [a]	0.17	−1.45	−1.68
	C_6F_5	−0.51	−1.56 [b]	−1.69
	C_6F_4H [d]	−0.55	−1.66 [e]	−1.68
	C_6H_5 [c]	−0.76		
$TpCF_3PP$	Cl^- [a]	0.25	−1.37	−1.62
	C_6F_5	−0.41	−1.55 [b]	−1.65
	C_6F_4H	−0.45		−1.73 [f]
	C_6H_5	−0.61		

[a] The Cl^- ligand of (P)FeCl is replaced by py to give $[(P)Fe(py)_2]^+$ in solution (see text). [b] Peak potential at 0.1 V/s. [c] From ref 15. [d] Recorded at 0.2 V/s. [e] Peak potential at 0.2 V/s. [f] Peak potential of two-electron transfer for overlapped waves II and III.

The first reduction of $(TpCF_3PP)Fe(C_6F_4H)(py)$ and $(TpCF_3PP)Fe(C_6F_5)(py)$ (reaction I) is reversible in pyridine by routine cyclic voltammetry (see dashed lines in Figure 3c,d) and occurs at $E_{1/2} = -0.45$ V (R = C_6F_4H) or −0.41 V (R = C_6F_5). Singly reduced $[TpCF_3PP)Fe(C_6F_4H)(py)]^-$ is more stable than single reduced $[TpCF_3PP)Fe(C_6F_5)(py)]^-$, and an additional electroreduction is not observed until $E_p = -1.75$ V, at which point an overall two-electron addition occurs to give $[(P)Fe]^{2-}$ as a final electroreduction product. The current for this process is double that of the first reduction (see solid line in Figure 3c), and the reduction most likely occurs via an ECE mechanism, where E represents a one-electron transfer and C a chemical reaction such as cleavage of the metal–carbon bond.

The electrogenerated product produced after reduction of $(TpCF_3PP)Fe(C_6F_4H)(py)$ at potentials more negative than −1.75 V undergoes two reversible one-electron oxidations at $E_{1/2} = -1.37$ and −1.62 V in pyridine (see dashed line in Figure 3c). These values are identical with $E_{1/2}$ values recorded for the second and third reduction of $(TpCF_3PP)FeCl$ under the same solution conditions (reactions II and III in Figure 3a) and indicate a loss of the σ-bonded axial ligand. The perfluorophenyl axial ligand is also lost after reduction of $(TpCF_3PP)Fe(C_6F_5)(py)$, but this reaction occurs after the addition of two electrons, as indicated by the formation of a $[(P)Fe]^-$ reduction wave on the first potential sweep (see solid line in Figure 3d).

Cyclic voltammograms of representative $(P)Fe(C_6F_4H)(py)$ and $(P)Fe(C_6F_5)(py)$ derivatives are shown in Figure 4. The reductions of $(TpCF_3PP)Fe(C_6F_5)(py)$, $(TpCF_3PP)Fe(C_6F_4H)(py)$, and $(TmTP)Fe(C_6F_4H)(py)$ are well-defined, and the Fe–carbon bond of the singly reduced species is stable, as indicated by the ratio of anodic to cathodic peak currents, i_{pa}/i_{pc}, which is approximately equal to 1.0. The i_{pa}/i_{pc} ratio is much smaller than 1.0 for $(TmTP)Fe(C_6F_5)(py)$ and $(TpTP)Fe(C_6F_5)(py)$ (figure not shown), and this is consistent with formation of a bis(pyridine)iron(II) reduction product on the cyclic voltammetry time scale.

Both $[(TpCF_3PP)Fe(C_6F_4H)(py)]^-$ and $[(TpCF_3PP)Fe(C_6F_5)(py)]^-$ are relatively stable in pyridine on the routine cyclic voltammetry time scale, and this contrasts with the five- or six-

(35) Bottomley, L. A.; Kadish, K. M. *Inorg. Chem.* **1981**, *20*, 1348.
(36) Kadish, K. M. *Prog. Inorg. Chem.* **1986**, *34*, 435–605.
(37) Kadish, K. M. In *Iron Porphyrins*; Lever, A. B. P., Gray, H. B., Eds.; Addison-Wesley: Reading, MA, 1983; Part II, Chapter 4.

Table V. Formation Constants for the Addition of Pyridine to (P)Fe(R) and $[(P)Fe(R)]^-$ in Benzonitrile Containing 0.2 M $TBA(PF_6)$[a]

	porphyrin, P				
		TPP		$TpCF_3PP$	
ax ligand, R	OEP log β^o	log β^o	log β^{-}[b]	log β^o	log β^{-}[b]
C_6H_5	1.6 ± 0.1[c]	2.5 ± 0.1		2.6 ± 0.1	
	(1.8 ± 0.2)[c]	(2.5 ± 0.2)[c]	(0.6 ± 0.2)[c]	(2.5 ± 0.2)[b]	(0.8 ± 0.2)
C_6F_4H	1.9 ± 0.1	3.1 ± 0.1		3.5 ± 0.1	
				(3.6 ± 0.2)[b]	(1.6 ± 0.2)
C_6F_5	2.0 ± 0.1	3.1 ± 0.1		3.5 ± 0.1	
		(3.2 ± 0.2)	(1.1 ± 0.2)	(3.6 ± 0.2)[b]	(1.6 ± 0.2)

[a] Unless indicated all values were calculated from spectrophotometric titration data. [b] Values in parentheses were calculated from electrochemical data. [c] Taken from ref 15.

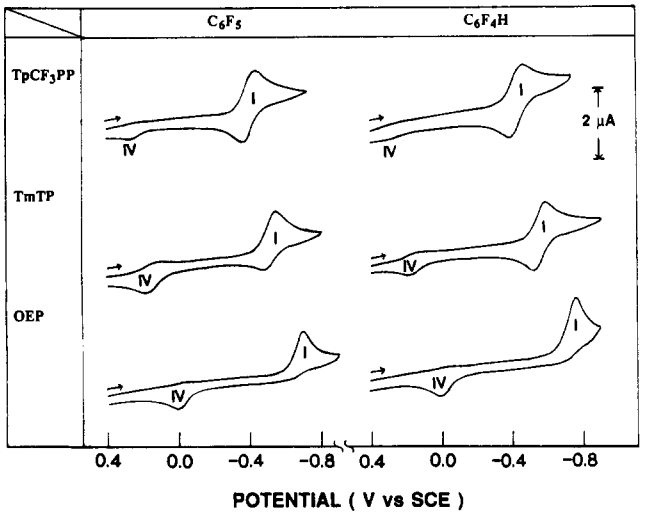

Figure 4. Cyclic voltammograms for the first reduction of representative (P)Fe(C_6F_4H)(py) and (P)Fe(C_6F_5)(py) complexes in pyridine containing 0.2 M $TBA(PF_6)$. Scan rate = 0.1 V/s.

coordinate $[(OEP)Fe(C_6F_5)]^-$ or $[(OEP)Fe(C_6F_4H)]^-$ complexes, all of which rapidly undergo an iron–carbon bond cleavage in either coordinating or noncoordinating media. The basicity of OEP is substantially larger than that of TpTP, TmTP, TPP, or $TpCF_3PP$, and irreversible reductions are invariably obtained for (OEP)Fe(C_6F_5)(py) and (OEP)Fe(C_6F_4H)(py), as shown in Figure 4. A bis(pyridine)iron(II) complex is formed after reduction of (OEP)Fe(C_6F_5)(py) or (OEP)Fe(C_6F_4H)(py), and neither $[(OEP)Fe(R)]^-$ nor $[(OEP)Fe(R)(py)]^-$ (R = C_6F_5, C_6F_4H) is observed on the cyclic voltammetry time scale.

The stability of given reduced complex does not appear to depend upon the potential for electroreduction, since (OEP)Fe(C_6F_4H)(py) (which is irreversibly reduced) and (TPP)Fe(C_6H_5)(py) (which is reversibly reduced) both undergo an initial one-electron addition at −0.76 ± 0.1 V (see Table IV). The stability of the reduced product does, however, appear to depend upon the macrocycle, since complexes with the more basic OEP macrocycle are all irreversibly reduced, as shown in Figure 4. The high-spin (OEP)Fe(R) derivatives are converted to low-spin (OEP)Fe(R)(py) in neat pyridine (see earlier section), but each compound loses the σ-bonded ligand upon addition of one electron and the formation of an Fe(II) porphyrin complex.

The reduction of (P)Fe(R)(py) can lead to either five- or six-coordinate complexes depending upon the concentration of pyridine in solution and the specific binding constant for pyridine addition to $[(P)Fe(R)]^-$. $[(OEP)Fe(C_6H_5)]^-$ does not coordinate pyridine in pyridine/benzonitrile mixtures,[15] but $[(TPP)Fe(C_6H_5)]^-$ is converted to $[(TPP)Fe(C_6H_5)(py)]^-$ in solutions containing a [py]/[porphyrin] ratio greater than 2000. The calculated formation constant for this reaction is log β = 0.6 ± 0.2.[15]

The reduction of $(TpCF_3PP)Fe(R)(py)$, where R = C_6F_5, C_6F_4H, or C_6H_5, may result in the formation of a six-coordinate complex, but this will depend upon the specific pyridine concentration in solution. This is shown in Figure 5, which presents diagnostic plots of $E_{1/2}$ for the first reduction of $(TpCF_3PP)Fe(C_6F_5)(py)$ vs log [py]. The plot has two components. The first has a theoretical Nernstian slope of −58 ± 5 mV for $\Delta E_{1/2}/\Delta$log [py] and is consistent with the loss of one pyridine ligand upon reduction, as shown in eq 2.

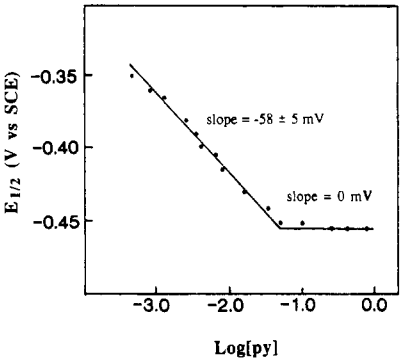

Figure 5. Diagnostic plots of $E_{1/2}$ vs log [py] for the first reduction of $(TpCF_3PP)Fe(C_6F_5)(py)$ in pyridine/benzonitrile mixtures containing 0.1 M $TBA(PF_6)$.

$$(TpCF_3PP)Fe(R)(py) + e^- \rightleftharpoons [(TpCF_3PP)Fe(R)]^- + py \quad (2)$$

The second component of the plot in Figure 5 has a $\Delta E_{1/2}/\Delta$log [py] slope of 0 mV, and this indicates that the pyridine ligand remains coordinated after electroreduction. Under these solution conditions, the overall electrode reaction is given by eq 3.

$$(TpCF_2PP)Fe(R)(py) + e^- \rightleftharpoons [(TpCF_3PP)Fe(R)(py)]^- \quad (3)$$

Pyridine binding constants for both $(TpCF_3PP)Fe(R)$ and $[(TpCF_3PP)Fe(R)]^-$ were calculated from data of the type given in Figure 5, and these results are presented in Table V, which also lists log β^0 for pyridine binding to the neutral compounds as calculated by UV–visible spectroscopy under the same solution conditions. As seen in the table, the electrochemically and spectrally calculated values are identical within experimental error.

Binding constants for pyridine addition to the low-spin (P)Fe(C_6H_5) complexes are smaller than those for addition to the high-spin C_6F_5 or C_6F_4H derivatives. The values of log β^0 also decrease by 1–2 orders of magnitude with increased basicity of the porphyrin ring (see Table V). This decrease may be due to the different spin states of compounds in the C_6H_5 and C_6F_5 or C_6F_4H series or alternatively to differences in electron density at the metal center that result from the different σ-bonded axial ligands of the (P)Fe(R) complexes. However, in either case, the stability of the iron–carbon bond upon reduction of (P)Fe(R)(py) appears to be related to the pyridine binding constant of (P)Fe(R) or $[(P)Fe(R)]^-$. The highest binding constants are obtained for $(TpCF_3PP)Fe(R)$ and $[(TpCF_3PP)Fe(R)]^-$, and the stability of the iron–carbon bond in reduced, six-coordinate complexes decreases according to the following order of macrocycles: $TpCF_3PP$ > TPP ≈ TmTP ≈ TpTP > OEP.

The first one-electron reduction of each $(TpCF_3PP)Fe(R)(py)$ species is reversible by routine cyclic voltammetry (see Figure 3), but the rate for conversion of $[(TpCF_3PP)Fe(R)(py)]^-$ to $(TpCF_3PP)Fe(py)_2$ is easily obtained from thin-layer cyclic voltammograms of the type shown in Figure 6. Process I in this

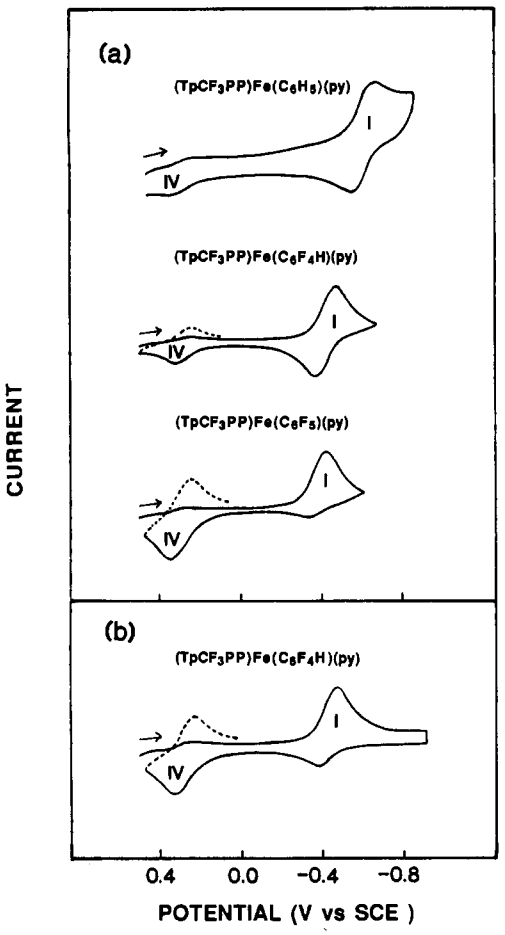

Figure 6. Thin-layer cyclic voltammograms of (a) $(TpCF_3PP)Fe(C_6H_5)$, $(TpCF_3PP)Fe(C_6F_4H)$, and $(TpCF_3PP)Fe(C_6F_5)$ and (b) $(TpCF_3PP)Fe(C_6F_4H)$ with holding at −0.90 V for 4 min in pyridine, 0.2 M TBA(PF_6). Scan rate = 10 mV/s.

figure corresponds to the reduction of $(TpCF_3PP)Fe(R)(py)$ at $E_{1/2}$ = −0.45 and −0.69 V, while process IV corresponds to the oxidation of $(TpCF_3PP)Fe(py)_2$ at $E_{1/2}$ = 0.25 V. The stability of $[(TpCF_3PP)Fe(R)]^-$ can be monitored by the ratio of the anodic to cathodic peak current, i_{pa}/i_{pc}, for process I, and the Fe–R stability decreases in the order $C_6H_5 > C_6F_4H > C_6F_5$.

Electrogenerated $[(TpCF_3PP)Fe(C_6F_4H)(py)]^-$ is stable for short periods of time on the thin-layer spectroelectrochemical time scale, and a ratio of $i_{pa}/i_{pc} \approx 0.7$ is obtained at a scan rate of 10 mV/s for a switching potential of −0.70 V. On the other hand, a cleavage of the iron–carbon bond is almost complete for the reduced complex under conditions where the potential is held at −0.90 V for a period of 240 s and then reversed. This is shown by the thin-layer cyclic voltammogram in Figure 6b, which has an i_{pa}/i_{pc} ratio of 0.3. The data in this figure suggest that UV–visible spectrum of $[(TpCF_3PP)Fe(C_6F_4H)(py)]^-$ should be obtained on short time scales and that the overall reduction proceeds according to the reaction sequence given in eq 4. This is indeed

$$(TpCF_3PP)Fe(R)(py) + e^- \rightleftharpoons [(TpCF_3PP)Fe(R)(py)]^- \rightarrow (TpCF_3PP)Fe(py)_2 \quad (4)$$

the case. During controlled-potential reduction of $(TpCF_3PP)Fe(C_6F_4H)(py)$ at −0.70 V, there is a decrease of intensity in the initial bands at 426 and 628 nm and the appearance of new bands at 446 and 534 nm. The shifts in wavelength during this reduction are similar to shifts obtained during reduction of $(TpCF_3PP)Fe(C_6H_5)(py)$ or $(TPP)Fe(C_6H_5)(py)$, and final spectral data for these single reduced complexes are all summarized in Table I.

The C_6F_4H ligand remains coordinated to the Fe(II) atom of $[TpCF_3PP)Fe(C_6F_4H)(py)]^-$ for short periods of time, but a cleavage of the iron–carbon bond occurs at longer electrolysis times. This results in the formation of an Fe(II) complex that is characterized by new bands at 425 and 530 nm. The final spectrum after controlled-potential electrolysis at longer time scales is identical with the spectrum of $(TpCF_3PP)Fe(py)_2$, which can be obtained by electroreduction of $[(TpCF_3PP)Fe^{III}(py)_2]^+$ in pyridine at 0.0 V.

In summary, (P)Fe(R)(py) may be reduced by one electron to give $[(P)Fe(R)(py)]^-$, $[(P)Fe(R)]^-$, or $(P)Fe(py)_2$, as shown by eq 2–4. The exact reduction product will depend upon the specific porphyrin macrocycle and axial ligand as well as upon the concentration of pyridine in solution. The reduction product may also depend upon the spin state of the electrogenerated Fe(II) species. For example, $[(P)Fe(R)(py)]^-$ should contain low-spin-state Fe(II), while $[(P)Fe(R)]^-$ and (P)Fe(py) should contain Fe(II) in a high spin state. Attempts are now underway to isolate several of these derivatives for further characterization.

Acknowledgment. The support of the National Institutes of Health (K.M.K., Grant GM 25172), the National Science Foundation (Grant INT-8412696), and NATO (Grant 0168/87) is gratefully acknowledged.

Registry No. $(TpCF_3PP)Fe(C_6H_5)$, 132125-45-2; $(TpCF_3PP)Fe(C_6F_4H)$, 132125-46-3; $(TpCF_3PP)Fe(C_6F_5)$, 132125-47-4; $(OEP)Fe(C_6H_5)$, 83614-06-6; $(OEP)Fe(C_6F_4H)$, 96482-32-5; $(OEP)Fe(C_6F_5)$, 96502-36-2; $(TPP)Fe(C_6F_5)$, 96502-37-3; $(TmTP)Fe(C_6F_5)$, 96502-38-4; $(TpTP)Fe(C_6F_5)$, 96532-02-4; (OEP)FeCl, 28755-93-3; (TpTP)FeCl, 19496-18-5; (TmTP)FeCl, 52155-49-4; (TPP)FeCl, 16456-81-8; $(TpCF_3PP)FeCl$, 101954-97-6; $(OEP)Fe(C_6F_5)(py)$, 132125-48-5; $(OEP)Fe(C_6F_4H)(py)$, 132125-49-6; $(OEP)Fe(C_6H_5)(py)$, 90148-87-1; $(TpTP)Fe(C_6F_5)(py)$, 132125-50-9; $(TpTP)Fe(C_6F_4H)(py)$, 132155-31-8; $(TmTP)Fe(C_6F_5)(py)$, 132155-32-9; $(TmTP)Fe(C_6F_4H)(py)$, 132125-51-0; $(TPP)Fe(C_6F_5)(py)$, 132125-52-1; $(TPP)Fe(C_6F_4H)(py)$, 132125-53-2; $(TPP)Fe(C_6H_5)(py)$, 90148-88-2; $(TpCF_3PP)Fe(C_6F_5)(py)$, 132125-54-3; $(TpCF_3PP)Fe(C_6F_4H)(py)$, 132125-55-4; $(TpCF_3PP)Fe(C_6H_5)(py)$, 132125-56-5; $(TPP)Fe(C_6H_5)$, 70936-44-6; $(TPP)Fe(C_6F_4H)$, 96482-33-6; $(TmTP)Fe(C_6H_5)$, 87607-83-8; $(TmTP)Fe(C_6F_4H)$, 96532-01-3; $(TpTP)Fe(C_6H_5)$, 87607-84-9; $(TpTP)Fe(C_6F_4H)$, 96482-34-7; phenylmagnesium bromide, 100-58-3; (2,3,5,6-tetrafluorophenyl)magnesium bromide, 40586-92-3; (pentafluorophenyl)magnesium bromide, 879-05-0.

Supplementary Material Available: A table listing ^1H NMR data for the (P)Fe(R) complexes, where P = TPP, TmTP, or TpTP and R = C_6H_5, C_6F_4H, or C_6F_5, in C_6D_6 and C_5D_5N and a figure showing ^1H NMR spectra of $(TpCF_3PP)Fe(C_6H_5)$ at 294 K in C_6D_6 and C_5D_5N (4 pages). Ordering information is given on any current masthead page.